Observation of a new high-β and high-density state of a magnetospheric plasma in RT-1

H. Saitoh*, Y. Yano, Z. Yoshida, M. Nishiura, J. Morikawa, Y. Kawazura, T. Nogami, and M. Yamasaki
Graduate School of Frontier Sciences, The University of Tokyo,
5-1-5 Kashiwanoha, Kashiwa, Chiba 277-8561, Japan
(Dated: July 10, 2014)

A new high-β and high-density state is reported for a plasma confined in a laboratory magnetosphere. In order to expand the parameter regime of an electron cyclotron resonance heating (ECH) experiment, the 8.2 GHz microwave power of the Ring Trap 1 (RT-1) device has been upgraded with the installation of a new waveguide system. The rated input power launched from a klystron was increased from 25 to 50 kW, which enabled the more stable formation of a hot-electron high-β plasma. The diamagnetic signal (the averaged value of four magnetic loops signals) of a plasma reached 5.2 mWb. According to a two-dimensional Grad-Shafranov analysis, the corresponding local β value is close to 100 %.

PACS numbers: 52.70.-m, 52.55.-s, 94.30.cq

I. INTRODUCTION

A magnetospheric dipole field configuration [1] is an innovative confinement concept motivated by satellite observations in the Jovian magnetosphere [2]. It is characterized by high-β stability and excellent confinement properties [3]. Stable confinement of high-β plasmas has been demonstrated in dipole magnetic fields generated by levitated superconducting magnets in the Ring Trap 1 (RT-1) [4], the Mini Ring Trap (Mini-RT) [5], and the Levitated Dipole Experiment (LDX) [6, 7]. In the first series of experiments in RT-1 [8–11], a plasma has been generated by using an electron cyclotron resonance heating (ECH) with 8.2 and 2.45 GHz microwaves [11, 12]. In cases with 2.45 GHz heating, line averaged electron density $n_{\rm a}$ saturated around $1.5\times10^{17}\,{\rm m}^{-3}$, which was about two times higher than the cut-off density $n_{\rm c\,2.45GHz}=7.4\times10^{16}\,{\rm m}^{-3}$. In cases with 8.2 GHz heating, where $n_{\rm c\,8.2GHz}=8.3\times10^{17}\,{\rm m}^{-3}$, $n_{\rm a}$ did not saturate with an input microwave power below the previous rated value of $P_{\rm f}=25$ kW. A diamagnetic signal $\Delta\Psi$ also did not reach a saturation. Therefore the increase in the 8.2 GHz microwave power makes it possible to realize further high-density and high-β states. As well as to generate and understand an extremely high-β plasma in the dipole field, high density states are strongly needed for the efficient ion cyclotron resonance heating (ICH) in future experiments.

In previous ECH plasmas in RT-1, operation regimes were classified into three categories [12]. (i) When neutral gas pressure was relatively high (5 mPa $< P_{\rm n}$), a high density and low β plasma was generated. (ii) When $P_{\rm n}$ was relatively low (0.5 mPa $< P_{\rm n} <$ 5 mPa), the ratio of a hot electron component drastically increased, resulting in a low density and high β plasma. (iii) At further low filled gas pressure ($P_{\rm n} <$ 0.5 mPa), the plasma became unstable. In order to enhance stored energy and to realize extremely high-β states, further increase in hot electron density is needed. When the hot electron ratio exceeds approximately 40 %, on the other hand, a plasma in a dipole field is often unstable [13]. The existence of a considerable ratio of cold electrons can stabilize the plasma, which is easily realized by supplying sufficient amount of neutral gas. However, an increase in $P_{\rm n}$ drastically enhances the charge-exchange cooling effects and prevents the formation of a large amount of hot electrons. Therefore the parameter regime had significant limitations; The high-β state was not simultaneously realized with the high-density state. In order to solve this problem, in this study, we upgraded the microwave power launched from a klystron from 25 to 50 kW, which realized the new regime of the ECH plasma in RT-1. Experimental investigation on the new high-β state is reported.

II. EXPERIMENTAL SETUP

As shown in Fig. 1, RT-1 is a magnetospheric configuration generated by a levitated superconducting magnet. Inside the vacuum chamber, RT-1 has a Bi-2223 high-$T_{\rm c}$ superconducting magnet. The current center of the magnet is located at $r_{\rm c}=25$ cm on the $z=0$ cm plane. The dipole field magnet is levitated by using a feedback-controlled lifting magnet located at the top of the chamber. The nominal currents of the dipole field and lifting magnets are 250 kAT and 28.8 kAT. The magnetic surfaces of the separatrix configuration generated by the two magnets are shown in Fig. 1 (b) as thin lines. More detailed explanations on the device are presented in [5] and the references therein.

The ECH system of RT-1 consists of an 8.2 GHz klystron (100 kW, 1 s), a 2.45 GHz magnetron (20 kW, 2 s), and their transmission lines. The 8.2 GHz microwave power is transmitted into the vacuum chamber through an isolator and waveguides including directional couplers, DC breaks, vacuum windows, and launchers. As shown in the figure, a new waveguide was installed at the P6 port, in addition to the previous waveguide connected to the P7 port. The rated power of each of the waveguides is 25 kW, and the maximum input power from the klystron was increased from 25 to 50 kW. The isolator was also upgraded and its maximum input power was increased from 25 to 100 kW for further installation of transmission lines in the future. In the experiment reported here, the microwaves were injected with the O-mode.

*Present address: Max Planck Institute for Plasma Physics, Boltzmannstraße 2, D-85748 Garching, Germany

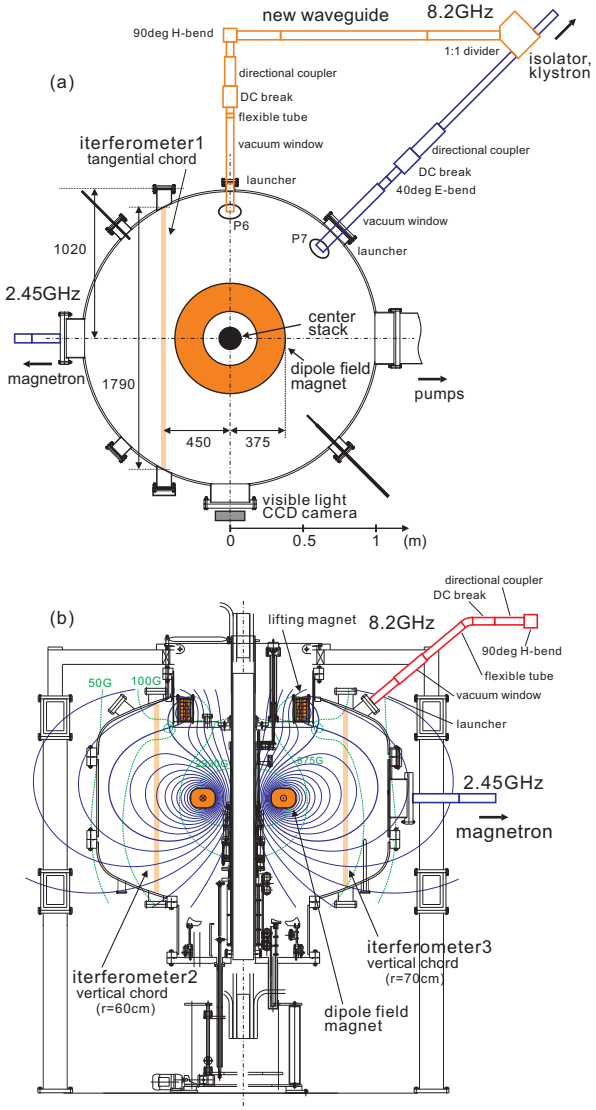

FIG. 1: (color online) (a) The top view and (b) poloidal projection of RT-1 including 8.2 GHz microwave waveguides. Interferometer chords are located at (1) tangential ports at $y = 45$ cm, (2) vertical ports at $r = 60$ cm, and (3) vertical ports at $r = 70$ cm. Thin lines show magnetic surfaces and contours of field strength generated by a levitating superconducting magnet and a lifting magnet.

The diamagnetic signal, or stored energy, of a plasma was measured with four magnetic loops winded outside of the vacuum chamber and Hall probes located inside the chamber. Based on these magnetic measurements, plasma equilibrium was reconstructed by a two-dimensional Grad-Shafranov analysis [14]. Line integrated electron densities n_l were measured by three 75 GHz ($\lambda = 4$ mm) heterodyne interferometers located (1) at a tangential chord at $y = 45$ cm, (2) at a vertical chord at $r = 60$ cm, and (3) at another vertical chord at $r = 70$ cm, as shown in Fig. 1. As discussed later, the spatial density profiles of a plasma were estimated by using the three chord interferometry. For the measurement of density fluctuations, a 4 GHz reflectometer is installed in the south-west port on the equator ($z = 0$ cm) of the device.

III. EXPERIMENTAL RESULTS AND DISCUSSION

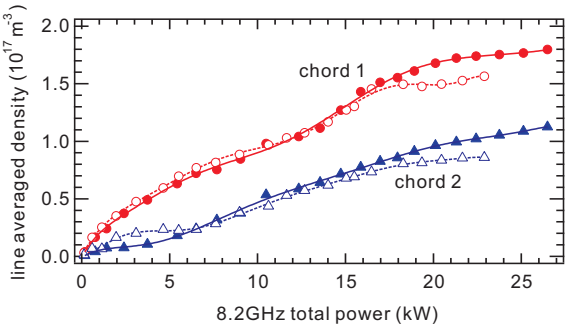

FIG. 2: (color online) Line averaged densities measured by the interferometer 1 (circles), n_{a1}, and by the interferometer 2 (triangles), n_{a2}, at various 8.2 GHz microwave power before (open) and after (close) the installation of a new isolator and a waveguide.

In Fig. 2, electron line averaged densities n_{a1} and n_{a2} are compared before and after the installation of the isolator and waveguide, in order to evaluate the variation of the transmission efficiency of a microwave due to the upgrade of the 8.2 GHz system. The filling gas pressure of hydrogen was $P_n = 2.5$ mPa for both of the cases. The superconducting magnet was mechanically supported in these experiments and the plasma was generated in a pure dipole magnetic field. As shown in the figure, we found no significant changes in electron densities measured both at the tangential port (chord 1) and at the vertical port (chord 2). There were no significant differences in line densities before and after the waveguide installation for similar P_f, also when the superconducting magnet was levitated. Therefore there is no significant increase in the loss of microwave power in the newly installed transmission line. When injection power exceeded approximately 18 kW, there were slight increases in n_{a1} and n_{a2} after the installation of the new waveguide system. It is possible that the formation efficiency of a plasma was improved by changing the number of the microwave injection ports from one to two.

Figure 3 plots the diamagnetic signals $\Delta\Psi$ and electron line averaged densities (n_{a1} and n_{a2}) versus injected microwave power P_f of 8.2 GHz for various neutral gas pressures P_n. Here $\Delta\Psi$ is the averaged value of four magnetic loop signals. As shown in Fig. 3 (a), when P_n is low (2.5 and 5.0 mPa), the stored energies of a plasma were relatively large even at low P_n. This is because the plasma had a considerable ratio of hot electrons in these conditions due to small charge-exchange cooling effects. In the previous experiments where P_f was limited below 25 kW, hot electron populations were greatly reduced by rising P_n. As shown in the figure, stored energies were very small at low P_f when $P_n = 10$, 12.5, and 15 mPa. However, an increase in P_f enabled the formation of a hot-electron high-β plasma even in a high P_n region. As shown in the figure, the transition from a low-β state to a high-β state is accompanied by increases in both stored energy and electron density. There was a small jump of $\Delta\Psi$ at $P_f = 22$ kW when $P_n = 5$ mPa. When $P_n = 10$ mPa, $\Delta\Psi$ drastically increased from 0.4 to 3.2 mWb at $P_f = 22$ kW. When $P_n = 12.5$ mPa, the

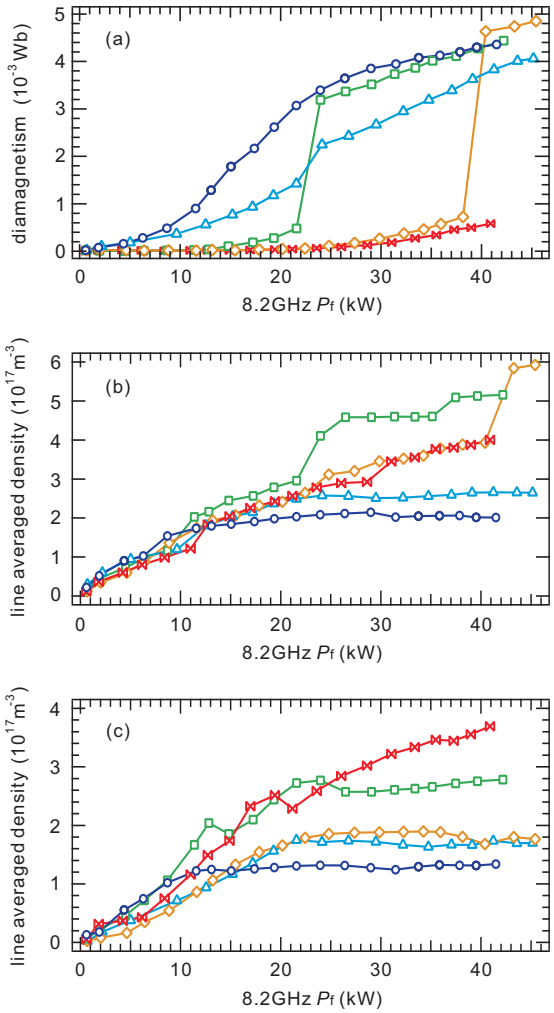

FIG. 3: (color online) (a) A diamagnetic signal (the averaged values of four loop signals) and line averaged densities (b) measured at chord 1, n_{a1} , and (c) measured at chord 2, n_{a2}, in variation of 8.2 GHz microwave power. Neutral gas pressure was 2.5 mPa (○), 5 mPa (△), 10 mPa (□), 12.5 mPa (◇), and 15 mPa (⋈).

transition appeared at $P_f = 38$ kW and $\Delta\Psi$ changed from 0.7 to 4.7 mWb. By increasing neutral gas pressure higher than $P_n = 15$ mPa, the transition was not observed and the plasma stayed in the low-β state in the present 8.2 GHz microwave power range. The β values of a plasma observed after the transition at high P_n cases are often higher than those with low P_n conditions.

As shown in Fig. 3 (b) and (c), n_{a1} and n_{a2} reached saturations at low neutral gas pressure of $P_n = 2.5$ and 5.0 mPa. In these formation conditions, the ratio of hot electron component in the plasma is extremely high and it often exceeds 40 %. Then the plasma sometimes becomes unstable and difficult to be generated stably [13]. Previously reported high-β plasma states were generated in this parameter region ($P_n < 5$ mPa) [12] except that P_f was limited below 25 kW. On the other hand, in the new high-β state realized at relatively high P_n conditions (> 10 mPa), the electron density steadily increased above $P_f = 25$ kW as shown in the figure. For a similar diamagnetic signal of $\Delta\Psi = 4.0$ mWb, n_{a1} when $P_n = 12.5$ mPa was twice as high as that of when $P_n = 2.5$ mPa and it reached $n_{a1} = 5 \times 10^{17}$ m^{-2}. The new high-β state is more stable than the previous high-β state, because electrons have a sufficient cold component together with the hot component. Thus the upgrade of the microwave system has significantly expanded the generable parameters of a plasma in RT-1.

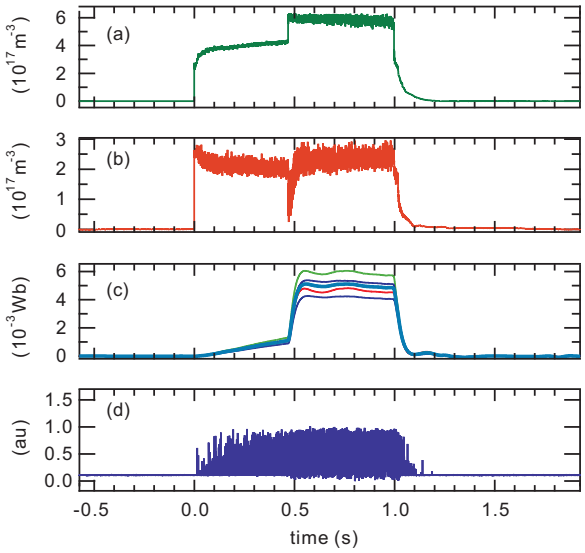

FIG. 4: (color online) Waveforms when the typical low and high β states were observed in one plasma formation period. The panels show (a) n_{a1}, (b) n_{a2}, (c) magnetic loop signals (the bold line shows the averaged value of four loop signals), and (d) an x-ray signal measured by a Si(Li) detector.

Figure 4 shows the waveforms of a plasma when the transition from low to high β states was observed in one formation period. The pressure of neutral gas was $P_n = 12.5$ mPa. A 8.2 GHz microwave of $P_f = 40$ kW was injected from $t = 0.0$ to 1.0 s. Initially, the plasma had relatively small $\Delta\Psi$ and high electron density, which are the typical parameters of a low-β plasma at high P_n regime. While $\Delta\Psi$ increased gradually in this period, the main component of electrons was a cold component. There was a transition to a high-β state at $t = 0.47$ s. As shown in Fig. 4 (c), $\Delta\Psi$ jumped from 1.2 to 5.0 mWb after the transition. At the same time, increases in electron line densities were observed especially in n_{a1} measured at the tangential port. The variation of n_{a2} measured at the vertical port was relatively small. The similar behaviors of n_{a1} and n_{a2} before and after the transition were also observed in Fig. 3 (b) and (c). As shown in Fig. 1, the chord 1 passes through the core region, while the chord 2 is located at the edge confinement region of a plasma. Therefore these observations indicate that a significant increase in electron density was realized after the transition in a strong field region near the dipole field magnet. We found that the transition characteristics show a strong hysteresis on the variation of P_n. The threshold values of P_n for the transition when increasing P_n were higher than those when decreasing P_n. The hysteresis becomes prominent when a working gas was hydrogen rather than helium, where storage effects are relatively strong. While further studies on

the behaviors of neutral particles are needed, these observations may suggest that the transition is caused by the transient effects of neutral particle recycling especially on the surface of the superconducting dipole field magnet.

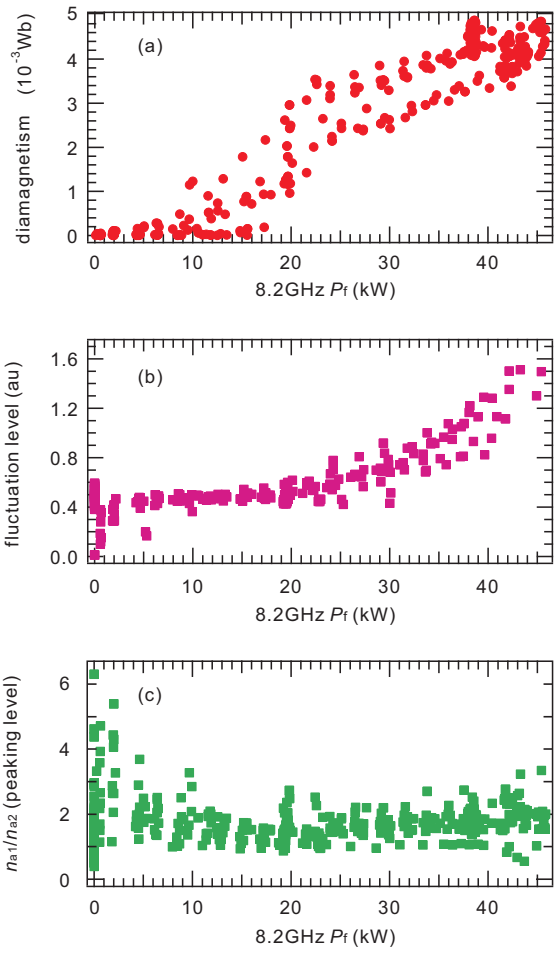

FIG. 5: (color online) (a) A diamagnetic signal $\Delta\Psi$, (b) a density fluctuation level measured by a reflectometer, and (c) the ratio of line averaged densities measured at chord 1 and 2.

The characteristics of a plasma from low to high β states were investigated by controlling the stored energy. In order to generate a plasma in similar conditions, the 8.2 GHz microwave was solely injected. Figure 5 shows (a) $\Delta\Psi$, (b) a density fluctuation level measured by a reflectometer, and (c) the ratio of line averaged densities n_{a1} and n_{a2}, in variation of P_f. Because an interferometer at the chord 1 mainly measures core electron density and another one at the chord 2 measures only edge density (Fig. 1), n_{a1}/n_{a2} gives the density peaking level of a plasma. On the spatial structure of a plasma, a more detailed analysis on the electron density profiles is discussed in the next section. When P_f exceeded 20 kW and $\Delta\Psi$ approached ~ 5.0 mWb, there was a distinct increase in the fluctuation level. Specific frequency peaks or clear mode structures were not observed in the analysis of frequency power spectrum of fluctuations. This is in marked contrast to the cases of unstable plasmas where the interchange mode was excited by the effects of hot electrons generated by ECH [13, 15]

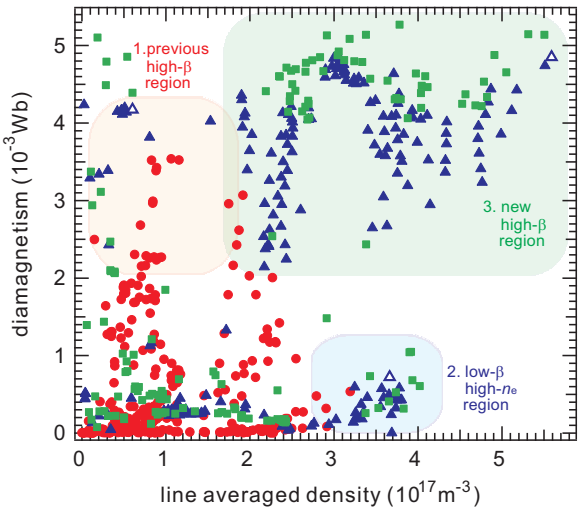

FIG. 6: (color online) Line averaged electron density measured at chord 1, n_{a1}, and a diamagnetic loop signal $\Delta\Psi$ when 8.2 GHz microwave power was $P_f < 25$ kW (circles) and when 25 kW $< P_f$ (triangles). Open triangles show data sets analyzed in the next section. Data for two-frequency heating at 8.2 and 2.45 GHz (25 kW $< P_f$) are also plotted (squares).

or where the interchange mode was centrifugally driven [16]. In fact, significant increase in the density peaking level was not observed in high-β plasmas when compared with low-β plasmas, as shown in Fig. 5 (c). A small rise of n_{a1}/n_{a2} at large P_f corresponds to the core density increase observed after the transition as shown in Fig. 4. The peaking levels after the transition were still smaller than those observed in small P_f cases.

Figure 6 plots previous and new parameter regimes of a plasma on the electron density-diamagnetism plane. The previous ($P_f < 25$ kW) high β plasmas were generated when neutral gas pressure P_n was relatively low. In this parameter regime, the plasma is often unstable due to the effects of excess of hot electrons. An increase in the microwave power enabled the formation of a stable high-β plasma at a relatively high density region. By changing formation conditions, including the two-frequency heating at 8.2 and 2.45 GHz microwaves with total injection power of $P_f = 64$ kW, the largest diamagnetic signal $\Delta\Psi$ (the averaged value of four loop signals) obtained was 5.2 mWb. According to the numerical calculation of a two-dimensional Grad-Shafranov analysis [14], the corresponding maximum local β value is close to 100 % near the pressure peak position.

We reconstruct the density profiles of a plasma according to the three-chord interferometry by using a simple model including the relativistic correction for the hot electron component [17–19]. Here we assume that the plasma density has a power-law dependence on r as

$$n_{z=0}(r) = n_0 r^{-a} \quad (1)$$

on the equator ($z = 0$ m, $r_c < r$) plane, where n_0 and a are constants, and it is a function of the magnetic surface. In the dipole magnetic field, charged particles *diffuse inward* [11]

until a peaked density profile in the real space is spontaneous generated. Therefore the density profile should primarily depend on the magnetic surface function. The mirror trap effects in the strongly inhomogeneous field are also important, especially in the cases of ECH plasmas where electrons are heated in the perpendicular direction. We also assume that electron density on a same magnetic surface is given by

$$n(r,z) = n_{z=0}(r) \times \left(\frac{B(r,z)}{B_0} \right)^{-b}, \qquad (2)$$

where $B(r,z)$ is a magnetic field strength and B_0 is the weakest field strength on the same magnetic surface. Here a is the peaking level of a density profile and b is the strength of mirror trap effects. We also assume that the plasma is axially symmetric. By using the values of line densities measured at the three chords, n_{l1}, n_{l2}, and n_{l3}, we find the values of a and b by the least-square method. We used a typical electron temperature $T_e = 50$ keV of a high-β plasma and ratios of hot electron population inferred from interferometry data [12] for the calculation of relativistic correction. A more detailed explanation on the reconstruction method will be reported elsewhere.

		case 1	case 2	case 3
P_n (mPa)		1.0	15	15
P_f (kW)		38	43	45
$\Delta\Psi$ (mWb)		4.2	0.7	4.9
chord 1	n_{a1} (m^{-3})	2.4×10^{17}	4.1×10^{17}	6.8×10^{17}
	r_{hot}	0.47	0.12	0.56
chord 2	n_{a2} (m^{-3})	1.1×10^{17}	3.4×10^{17}	3.7×10^{17}
	r_{hot}	0.45	0.17	0.75
chord 3	n_{a3} (m^{-3})	1.1×10^{17}	2.8×10^{17}	3.0×10^{17}
	r_{hot}	0.59	0.25	0.60
a		2.1	1.6	2.7
b		4.8	0.6	2.3

TABLE I: Experimental conditions and analysis results of interferometry. Neutral gas pressure P_n, microwave power P_f, diamagnetic signals $\Delta\Psi$, interferometer data including the relativistic correction, and the calculated values of a and b in cases with (1) high-β and low-n_e (a previously reported high-β region), (2) low-β and high-n_e (before the transition), and (3) high-β and high-n_e (after the transition) states, see Fig. 6.

Table I summarizes the analysis results for three typical parameter regimes of a plasma. The data shots used for the analysis are plotted in Fig. 6 as open triangles. Here the hot electron ratio r_{hot} was inferred from the ratio of slow decay component in the interferometer signals observed after terminating the microwave power [12]. The case 1 is a high-β and low-n_e state realized at low neutral gas pressure P_n, which has been realized since the past experiment. The cases 2 and 3 are both when P_n is relatively high. The case 2 is a relatively low-β state before the transition. The main component of electrons in this case is a cold component. The case 3 is the newly-reported high-β and high-n_e state observed after the transition. For various experimental conditions, the values of a and b are both positive, which is consistent with the self-organization of a peaked density profile in a strongly inhomogeneous dipole field configuration.

Figure 7 shows the density profiles of plasmas calculated by using the values of a and b in Table I for the three cases. As shown in Fig. 7 (1), in the high-β and low-n_e case, where the plasma mainly consists of hot electrons generated by ECH, the plasma shape is strongly influenced by mirror trap effects. The density profile is then strongly non-uniform on the magnetic surfaces. The high density plasma is located in a weak field region and the plasma expands toward the chamber wall. This result is consistent with the equilibrium analysis and also with the observation of strong x-ray emission on the chamber wall hit by hot electrons. In this case, the plasma has a large density gradient especially in the vertical direction. In contrast, when the ratio of cold electrons is high in the low-β and high-n_e case, as shown in Fig. 7 (2), mirror trap effects are relatively small. The shapes of the density contours are quite close to those of the magnetic surfaces. Finally, Fig. 7 (3) are the density profiles of the new high-β and high-n_e state observed after the transition. The mirror trap effects are again significant, but the density gradient along the magnetic surfaces is rather small when compared with the case 1, as a result of the increased electron density.

IV. SUMMARY

In order to expand the parameter regime of an ECH plasma experiment in RT-1, we upgraded the 8.2 GHz microwave system and increased the rated input power from 25 to 50 kW. An increase in the microwave power enabled the transition of a plasma to a new high-β and high-density state. In the new high-β state, a large amount of hot electrons were simultaneously generated with cold electrons, realizing a more stable formation of the hot-electron high-β plasma. When a plasma was generated with two-frequency heating at 8.2 and 2.45 GHz with a total input power of up to 64 kW, the diamagnetic signal (the averaged value of four magnetic oops signals) reached $\Delta\Psi \sim 5.2$ mWb. A two-dimensional Grad-Shafranov analysis showed that the corresponding local β value is close to 100 %, while the peaking level of a plasma did not significantly increase at the high-β region. However, according to a reflectometer measurements, the fluctuation level of a plasma significantly increased in very large $\Delta\Psi$ conditions. These observations may suggest that the plasma is still below the pressure driven instability limit and the fluctuation increased because the lowest field strength in a plasma approached to zero. It is noted that the optimization of the spatial profile of a plasma will realize further increase in the total stored energy of a plasma in future experiments. We also investigated the spatial structures of a plasma by using a three-chord interferometry including a relativistic correction for hot electrons. The measurements showed that the plasma has peaked density profiles and also strongly affected by the mirror trap of hot electrons in a weak field region, which is consistent with the self-organization of magnetized charged particles in a strongly inhomogeneous dipole magnetic field.

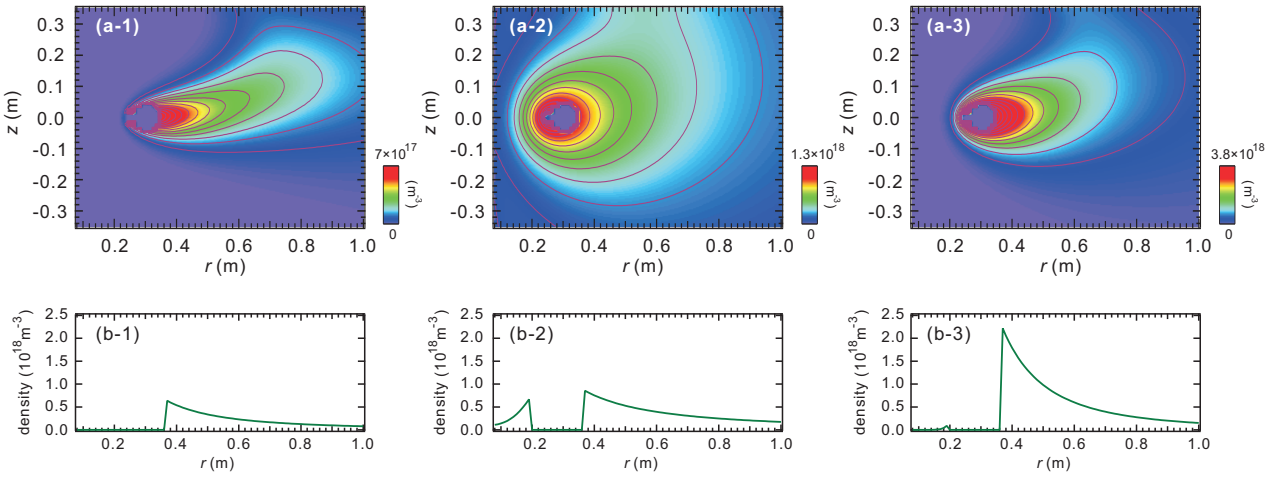

FIG. 7: (color online) Electron density profiles corresponding to Table I. (a) Two dimensional contour maps and (b) radial profiles on the $z = 0$ m plane of electron density in cases with (1) high-β and low-n_e, (2) low-β and high-n_e, and (3) high-β and high-n_e states. On the $z = 0$ m plane, the dipole field magnet surface is located at $r = 0.18$ and 0.375 m.

V. ACKNOWLEDGEMENT

This work was supported by Grants-in-Aid for Scientific Research (KAKENHI) No.23224014 from Japan Society for the Promotion of Science (JSPS). The authors are grateful to Professors Takashi Maekawa and Hiroshi Idei for giving valuable comments and advices.

[1] A. Hasegawa, Comm. Plasma Phys. Contr. Fusion **11**, 147 (1987).
[2] S. M. Krimigis, T. P. Armstrong, W. I. Axford, C. O. Bostrom, C. Y. Fan, G. Gloeckler, L. J. Lanzerotti, E. P. Keath, R. D. Zwickl, J. F. Carbary, and D. C. Hamilton, Science **206**, 977 (1979).
[3] A. Hasegawa, L. Chen, and M. E. Mauel, Nucl. Fusion **30**, 2405 (1990).
[4] Z. Yoshida, H. Saitoh, J. Morikawa, Y. Yano, S. Watanabe, and Y. Ogawa, Phys. Rev. Lett. **104**, 235004 (2010).
[5] Y. Ogawa, J. Morikawa, T. Mito, N. Yanagi, M. Iwakuma, H. Nihei, K. Ohkuni, D. Hori, S. Yamakoshi, I. Itoh, S. Nose, and T. Uede, J. Plasma Fusion Res. **79**, 643 (2003).
[6] D. T. Garnier, A. Hansen, M. E. Mauel, E. Ortiz, A. C. Boxer, J. Ellsworth, I. Karim, J. Kesner, S. Mahar, and A. Roach, Phys. Plasmas, **13**, 056111 (2006).
[7] A. C. Boxer, R. Bergmann, J. L. Ellsworth, D. T. Garnier, J. Kesner, M. E. Mauel, and P. Woskov, Nature Phys. **6**, 207 (2010).
[8] S. M. Mahajan and Z. Yoshida, Phys. Rev. Lett. **81**, 4863 (1998).
[9] Z. Yoshida and S. M. Mahajan, Phys. Rev. Lett. **88**, 095001 (2002).
[10] Z. Yoshida, Y. Yano, J. Morikawa, and H. Saitoh, Phys. Plasmas **19**, 072303 (2012).
[11] Z. Yoshida, H. Saitoh, Y. Yano, H. Mikami, N. Kasaoka, W. Sakamoto, J. Morikawa, M. Furukawa, and S. M. Mahajan, Plasma Phys. Cntrl. Fusion **55**, 014018 (2013).
[12] H. Saitoh, Z. Yoshida, J. Morikawa, Y. Yano, T. Mizushima, Y. Ogawa, M. Furukawa, Y. Kawai, K. Harima, Y. Kawazura, Y. Kaneko, K. Tadachi, S. Emoto, M. Kobayashi, T. Sugiura and G. Vogel, Nucl. Fusion **51**, 063034 (2011).
[13] H. Saitoh, Z. Yoshida, J. Morikawa, Y. Yano, H. Mikami, N. Kasaoka, and W. Sakamoto, Phys. Plasmas **19**, 064502 (2012).
[14] M. Furukawa, H. Hayashi, and Z. Yoshida, Phys. Plasmas **17**, 022503 (2010).
[15] H. P. Warren and M. E. Mauel, Phys. Plasmas **2**, 4185 (1995).
[16] B. Levitt, D. Maslovsky, and M. E. Mauel, Phys. Rev. Lett. **94**, 175002 (2005).
[17] I. H. Hutchinson, *Principles of Plasma Diagnostics, 2nd Edition*, Cambridge University Press (2002).
[18] E. Mazzucato, Phys. Fluids B **4**, 3460 (1992).
[19] H. Hojo, A. Mase, and K. Kawahata, Plasma Fusion Res. **4**, 010 (2009).